Room-Temperature Metal−Hydride Discharge Source, with Observations on NiH and FeH†

Raphaël Vallon,‡ Stephen H. Ashworth,§ Patrick Crozet,* Robert W. Field,‖ Damien Forthomme,⊥ Heather Harker, Cyril Richard, and Amanda J. Ross*

Université de Lyon, F-69622, Lyon, Université Lyon 1 & CNRS, UMR 5579 LASIM, 43 Bd du 11 novembre 1918, Villeurbanne, France

Received: April 13, 2009; Revised Manuscript Received: June 26, 2009

A metal sputtering source suitable for laboratory production of metal hydrides is described. Sputtering from pure nickel or iron in an Ar/H_2 discharge is analyzed at low resolution. High resolution laser excitation and dispersed fluorescence spectra of NiH have also been recorded. The source has been designed to operate with a ferromagnetic circuit for Zeeman spectroscopy. Signals from the source are strong enough to record dispersed fluorescence from NiH by Fourier transform interferometry in magnetic fields up to 1 T. We establish that FeH can also be formed in this source.

Introduction

Several transition metal oxides and hydrides have been observed in the spectra of cool stars and sunspots. Because of nonzero transition metal orbital and spin angular momenta, the magnetic response of these species offers a potentially useful probe of cool magnetized stellar atmospheres, notably by stellar spectropolarimetry.[1] This assumes that the Zeeman spectra of these species are known and understood. However, the complex electronic structures of these species require laboratory investigations to establish the often unclear magnetic response for individual rotational levels. Work at MIT in the early '90s focused on understanding the electronic structure of the low-lying doublet states of NiH. A "supermultiplet" model[2] emerged, which successfully modeled the data available at that time and gave much insight into some of the peculiar energy level patterns arising from interelectronic state coupling. No such model is available for the excited electronic states. Recent work in Lyon has aimed to extend observations on the low-lying (<1 eV) states of NiH, and to develop an experimental setup that could characterize Zeeman patterns in many ro-vibronic levels. A key point in this study was therefore to find a reliable, durable and efficient way of making MH radicals.

The constraints on this work are related to the mismatch between stellar atmospheric conditions and those possible in the laboratory. Temperatures of cool stars exceed 3000 K, with Boltzmann distributions far removed from those achievable under less extreme conditions. Doppler widths are about 3 times narrower close to room temperature than they are at stellar temperatures, making Zeeman patterns and other small splittings easier to resolve. That said, suitable observations need to be made far from the maximum of the Boltzmann distribution in the laboratory spectrum. High signal-to-noise ratios are therefore essential. We have shown[3] that Fourier transform spectra of dispersed laser-induced fluorescence in NiH, following excitation by a single (well-chosen) laser frequency, show many transitions to nonthermally populated levels, and that hundreds of lines can be recorded in a single spectrum. Our commercial FT interferometer works in "continuous scanning" mode, effectively taking data points in 12 ns windows at 26 μs intervals, and it requires good short-term stability from whatever light source is chosen. The internal absorption sources, for example, are stabilized to better than 0.5%. Dispersed laser-induced fluorescence, where a spectrum emerges from a black background, is less demanding in this respect than absorption sources, and spectra are routinely recorded with S/N levels around 20:1, working with thermally produced gas-phase samples. The discharge environment is more critical, as "occasional" fluctuations introduce many small spikes in the interferograms that cannot be readily recognized or eliminated prior to the Fourier transformations. Sparks or momentary extinctions of the discharge can sometimes corrupt the spectrum beyond repair. For high resolution spectra, recording times are of the order of hours, so the stability of the source is of particular importance.

Experimental Section

We have used a continuous DC discharge flow source to produce metal monohydride species in the presence of a magnetic field. A DC voltage (typically between 400 and 700 V) from a commercial stabilized power supply (MCN 700−1250 from FuG Elektronik GmbH) is applied through a 2.5 kΩ ballast resistor, achieving operating currents $I_{DC} = 100-180$ mA in the flow tube. Radicals formed in the discharge are excited by a single-mode, continuous wave (cw) dye laser and can be conveniently studied either in laser excitation or in dispersed fluorescence, the latter coupling laser-induced emission to a Fourier transform spectrometer (FTS). NiH was chosen as a prototype molecule because of its strong and well-characterized fluorescence in the orange-red. The discharge is placed over an interaction chamber, where the laser intersects the flow of products from the discharge. The gas mixture (10% H_2 in argon) flows continuously, at a rate of typically 60 standard cm^3/min (sccm), through the chamber, which is maintained at pressures between 0.5 and 2 Torr with a primary vacuum pump. The

† Part of the "Robert W. Field Festschrift".

* Corresponding authors. P.C., e-mail, crozet@lasim.univ-lyon1.fr; tel, +33 472448563; fax, (+33)427445871. A.J.R.: e-mail, ross@lasim.univ-lyon1.fr; tel, +33 472448256; fax, (+33)427445871.

‡ Current address: ONERA The French Aerospace Lab, DMPH-SLM Chemin de la Hunière et des Joncherettes, 91761 Palaiseau Cedex, France.

§ School of Chemical Sciences and Pharmacy, University of East Anglia, Norwich NR4 7TJ, U.K.

‖ Department of Chemistry, Massachusetts Institute of Technology, Cambridge, MA 02139.

⊥ Physics Department, University of New Brunswick, P.O. BOX 4400, Fredericton, New Brunswick, E3B 5A3 Canada.

10.1021/jp9033968 CCC: $40.75
Published on Web 07/15/2009

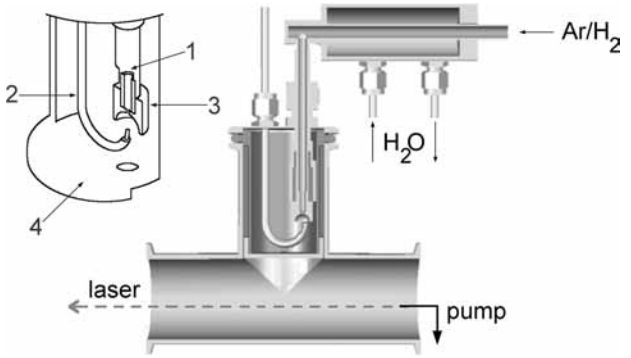

Figure 1. Schematic diagram showing a section through the T-shaped "hot" source, with an expanded view of the "tower". A partially hollowed, cylindrical cathode (3) screws directly onto the threaded, copper gas inlet tube (1), which is insulated from the housing by a larger glass tube. The copper needle anode (2) is insulated from the housing by Teflon tubing. The tip near the cathode is left bare. Sputtering products escape through a circular aperture in the light shield (4) located below the discharge.

chamber consists of a stainless steel tube (internal diameter 40 mm) with an outlet for evacuation located close to the Brewster window at one end.

Two designs for the sputtering source have been tested and compared.[4] The first design, which we shall call "hot source", replicated the original design from MIT.[5] It consists of a T-shaped flow tube (Figure 1), built from stainless steel sections, separated into two compartments: the "tower" and the "interaction chamber". The tower contains the hollow cathode sputtering source, surrounded by a light shielding box, which is painted black and has a hole in its lower section. Gas flows through the slit into the chamber. A water-cooling jacket was added around the copper gas inlet tube to cool the cathode that screws directly on to it. Both the gas inlet tube and the copper-needle anode are insulated from the housing by glass and Teflon tubes, respectively. The cathode is made of pure nickel (99.98%, Goodfellow). Different cylindrical cathode designs have been tested, with the lower part cut flat, or else partially hollowed out, with either a smooth or machine-roughened inner surface (intended to enhance sputtering). Best results were obtained with the simplest design: a flat-based cylinder (length = diameter = 12 mm), centrally pierced by a cylindrical hole (diameter = 2 mm) threaded for half its length. The performance of this system was not entirely satisfactory. Sputtering is fast, metal is worn away from the edges of the central hole in the cathode, and the discharge eventually becomes unstable. Worse, from the point of view of long-term signal stability, the production of radicals diminishes after a few minutes' operation, attaining a stable but low level of fluorescence. Initially, we thought this was due to degradation of the electrodes, or deposits on the windows, but it proved to be a thermal effect. If the source was allowed to rest for 30 min, the initial signal levels could be retrieved for a further 5−10 min.

Our second design (the "cold source") therefore incorporated a water-cooling arrangement for the cathode. A cooling tower, built from copper cylinders, surrounds the cathode, as shown in Figure 2. It incorporates a chicane-style water circuit to channel the water flow, to maximize cooling efficiency. A thin layer of high thermal conductivity clay is pasted onto the cathode to improve contact between the tower and the cathode. This arrangement cools the gas inside the interaction chamber and finally produces NiH radicals at around 300 K. The second design also implements a different design of anode. An annular anode, located 5−10 mm below the base of the cathode replaces

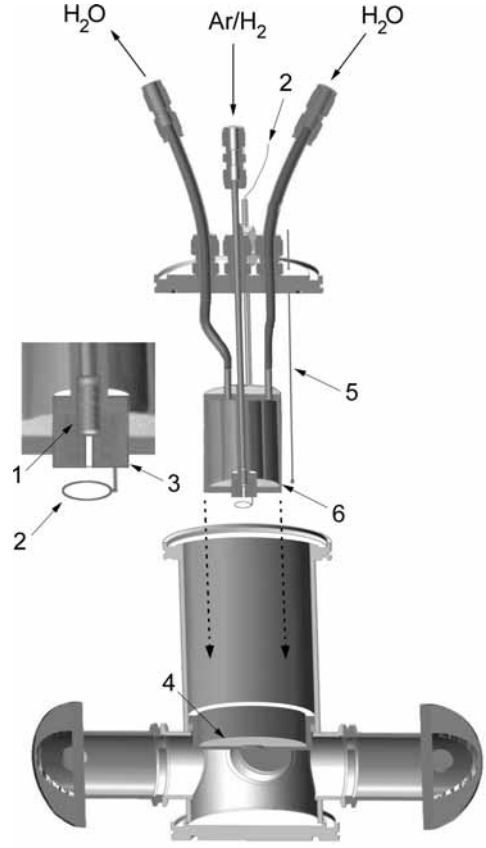

Figure 2. Schematic diagram showing a section through the "cold" source, with an expanded view of the anode/cathode region. The hollowed, cylindrical cathode (3) screws onto the threaded, copper gas inlet tube via a hollow set (grub) screw (1). An annular anode (2) is located below the cathode and channels the beam of sputtered gas phase species through a slit in the light shield (4). A copper chicane-style water circuit (6) provides efficient water cooling of the cathode. A thermocouple (5) is located outside the discharge. The discharge unit fits into the tower, sealed with an O-ring.

the pointed anode used before. It channels the beam of sputtered gas phase species, as reaction products flow (primarily) through the anode ring down to the zone where they can be excited with the laser. This source can be operated for many hours without significant loss of signal, and the electrodes need to be cleaned only after a few days' continual use. Eventually, the LIF signal decreases, because the sputtering process causes the cathode to be worn away. At first, the signal can be recovered by increasing the gas flow (without changing pressure), but eventually the discharge becomes unstable. Deposits on the Brewster windows also accumulate after 10 h or so operation, increasing the noise from laser scatter significantly. The lifetime of a worn cathode can be extended by coiling a narrow strip of nickel foil (we used 0.15 mm thickness) into the enlarged orifice; the foil needs replacing daily. We have ascertained that NiH can be readily produced by winding a thin strip of nickel into a worn copper cathode, which suggests an economical option if working with relatively expensive metals, avoiding the need to replace the entire cathode head.

Results

1. Low Resolution Spectrum of the Ni Discharge. A low resolution digital grating spectrometer (Avantes 2048, fwhm 4.3 nm) was used to record chemiluminescence from the discharge immediately below the anode, at the entrance of the interaction chamber. A typical spectrum, with relative intensities corrected

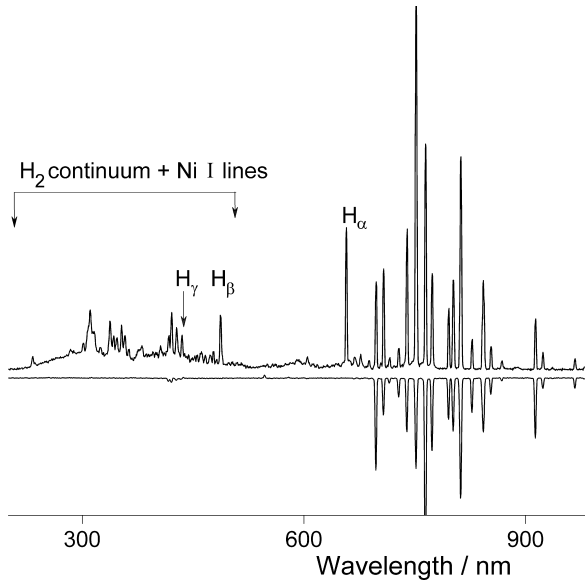

Figure 3. Low resolution emission spectrum from the "cold" source, and comparison with emission from an argon calibration lamp (lower trace).

for instrumental response, is shown in Figure 3. The NIST Atomic Spectra Database[6] has been used to identify the atomic species produced in the discharge region. From the UV to the green, the spectrum is dominated by neutral Ni emission lines, while from the red to the near-infrared, the strong features are from neutral Ar. The lower trace in Figure 3 shows the spectrum from an argon lamp. The strong blue-green jet seen by eye results from Ni I emission lines, the strong hydrogen Balmer H_β line at 486.1 nm and part of the H_2 continuum,[7] which lies in the region 160−500 nm. The first three Balmer lines can be identified in the spectrum, which proves that H_2 is efficiently dissociated by the discharge. The hydrogen features are well explained[8] by the following processes:

$$\mathrm{Ar}^* + \mathrm{H_2}(\mathrm{X}^1\Sigma_g^+) \rightarrow \mathrm{Ar} + \mathrm{H_2}(\mathrm{a}^3\Sigma_g^+) \quad (1)$$

$$\mathrm{H_2}(\mathrm{a}^3\Sigma_g^+) \rightarrow \mathrm{H_2}(\mathrm{b}^3\Sigma_u^+) + h\nu\,(\mathrm{continuum}) \quad (2)$$

$$\mathrm{H_2}(\mathrm{b}^3\Sigma_u^+) \rightarrow 2\mathrm{H}^\bullet \quad (3)$$

Process (1) occurs with a quasi-resonant match between the energies of Ar metastable states ($^3P_2$, $^3P_0$), and the $v' = 0$ level of the molecular hydrogen a $^3\Sigma_g^+$ state. Following (3), hydrogen atoms need then to be excited for instance by electron impact in the discharge to $n > 2$ to produce the observed Balmer lines.

2. Influence of H_2/Ar in the Sputtering Process. The Ph.D. thesis work of Gray at MIT mentioned an optimum ratio of 10% H_2 in argon for NiH production with the hot source,[9] but no detail was given. We investigated the sensitivity of NiH production to hydrogen content, on the assumption that the global LIF intensity signal is a good monitor of NiH formation, and confirm optimum performance for 8−12% [H_2]/Ar. The laser was tuned to the strongest line in the yellow region of the spectrum ($Q(2^1/_2)$ B $^2\Delta_{5/2}$ − X_1 $^2\Delta_{5/2}(1-0)$ at 17 462.96 cm^{-1} for ^{58}NiH), operating at a power of 150 mW to avoid saturation. A series of resolved fluorescence spectra was recorded under constant conditions of discharge and pressure (1 Torr, with gas flow controlled by a mass flow meter) using different relative

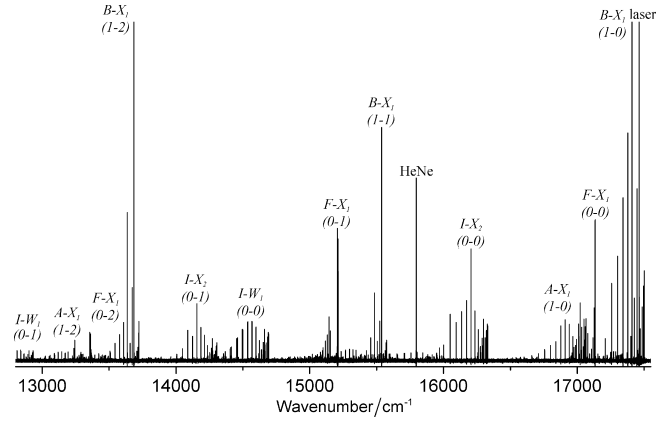

Figure 4. Fourier transform resolved fluorescence spectrum of ^{58}NiH, following laser excitation via $Q(2^1/_2)$ B−X_1 (1−0) at 17 462.94 cm^{-1}. All bands other than B−X_1 (1 −v'') result from collisionally induced electronic energy transfer. The line labeled "HeNe" comes from scattered light from the interferometer's internal calibration laser.

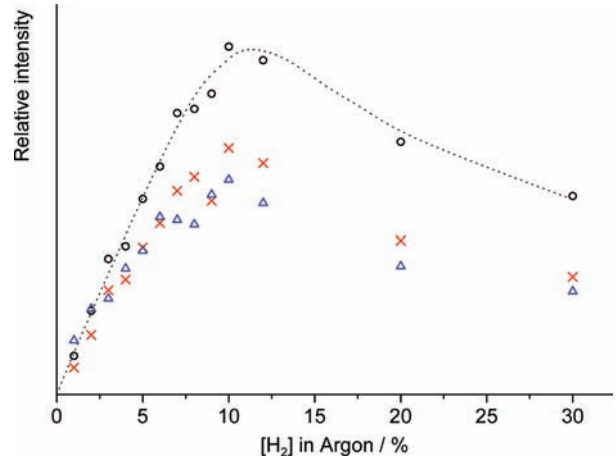

Figure 5. NiH fluorescence signals as a function of the relative concentration of hydrogen and argon. Open circles (○) indicate direct fluorescence, the broken line is intended only as a guide. Crosses (×) plot integrated intensities of fluorescence 14 000−14 700 cm^{-1} from I−X_2 $^2\Delta_{3/2}(0-1)$ and the I−W_1 $^2\Pi_{3/2}(0-0)$ bands, and open triangles (Δ) represent integrated intensities of the F $^2\Phi_{7/2}$−X_1 $^2\Delta_{5/2}(0-1)$ band from 15 000 to 15 200 cm^{-1}. Collisional signal intensities have been multiplied by 8 to illustrate them conveniently on the same graph.

concentrations of hydrogen in argon. Because we are investigating dispersed fluorescence, we can distinguish between emission from the excited state pumped directly by the laser, and emission following collisionally induced energy transfer (electronic energy transfer happens to be unusually strong in NiH,[3,10] as illustrated in Figure 4, where the strongest electronic transitions are identified). Figure 5 shows plots of the relative intensities of direct fluorescence ($P(3^1/_2)$ and $Q(2^1/_2)$ B $^2\Delta_{5/2}$−X_1 $^2\Delta_{5/2}(1-2)$ band), and for collisionally induced transitions from the I ($\Omega' = {}^3/_2$) and the F $^2\Phi_{7/2}$ states, for different H_2 concentrations. The relative intensities of direct and collisionally induced fluorescence increased linearly in mixtures up to 4% H_2, but as the H_2/argon ratio rose further, the collisionally induced bands increased in intensity a little less rapidly than the direct fluorescence. This is not unreasonable, as argon is the most probable collision partner for effective electronic energy transfer processes in this source. The absolute ratio of collisionally induced to direct fluorescence varies with the choice of laser frequency, being highest when there happen to be many quantum levels close to the one populated by the laser. We had expected

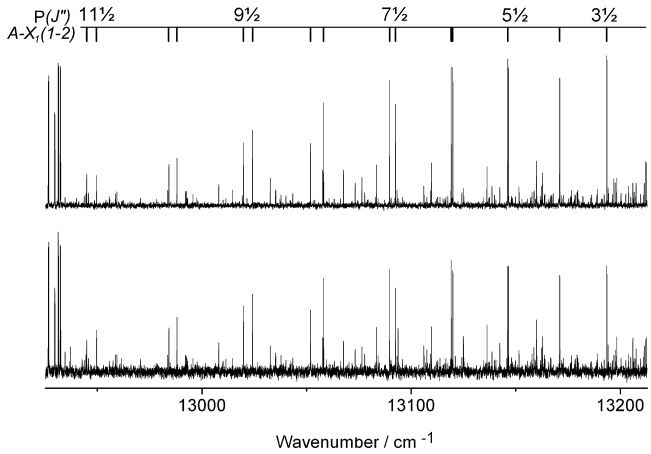

Figure 6. Comparison of the signal/noise ratio achieved in FT resolved fluorescence spectra taken with the "cold" source (upper trace) and "hot" source (lower trace), looking at one of the weakest regions (around 13 100 cm^{-1}) in Figure 4.

an initial linear dependence on hydrogen reflecting the production of NiH by reaction with sputtered nickel, but the *shape* of this curve, with sharp rise and slow decay, turns out to be very similar to the sputtering-efficiency curve measured for gold,[11] where contributions from both Ar^+ and ArH^+ result in a peak sputtering rate with H_2 concentrations around 10%. (The study on gold revealed a maximum contribution from Ar^+ at 10% H_2/Ar concentration, whereas that from ArH^+ peaked more slowly, at a much higher (50%) H_2/Ar ratio.) In all subsequent work, we worked with a mixture of 10% H_2 in argon.

3. High Resolution Spectra of NiH. Figure 6 illustrates the improvement in signal/noise ratio of dispersed fluorescence spectra achieved with the water-cooled cathode, looking at some collisionally induced transitions in one of the weaker parts of the spectrum. The J'' quantum numbers in Figure 6 refer to P lines in the $A-X_1(1-2)$ band. The upper spectrum was produced with the "cold" source, and the lower one with the hotter source. Both were recorded at an instrumental resolution of 0.05 cm^{-1} and were obtained after coaddition of 40 scans on a Bomem DA3 FT spectrometer. The discharge was operated at 446 V, 100 mA, at a pressure $P = 2.1$ Torr. The laser was tuned to the ^{58}NiH $Q(2^1/_2)$ $B-X_1(1-0)$ transition, with 400 mW laser power from a cw single-mode ring dye laser (Spectra-Physics 380D). The spectra are intensity-scaled to the stronger transitions on the left-hand side of the figure (R head, $I-W_1\ ^2\Pi_{3/2}(0-1)$ band). Rotational temperatures of 32 and 130 °C, respectively, have been deduced from independent (laser excitation) Doppler-width measurements with "cold" and "hot" sources. In this region of the spectrum, the signal/noise ratio is improved by a factor of 2.5 with equal recording times, so using the cooler source allows recording times to be reduced by a factor of 6 to achieve results of comparable quality. The improvement in S/N ratio achieved with the colder source is particularly appreciable in allowing the weaker features of the spectrum to emerge. We have thus extended the range of observations of levels of the lowest electronic states, particularly for low-lying excited states and for minor isotopes of nickel. Energy levels have now been mapped out (with conservatively estimated uncertainties of 0.015 cm^{-1}) up to $v'' = 4$ in the $X_1\ ^2\Delta_{5/2}$ ground state, 7500 cm^{-1} above the rotationless ground state level. Earlier literature reports[2] stopped at $J = 2^1/_2$, $v'' = 2$, $E = 3777.2$ cm^{-1} above the rotationless ground state. Observations of the $\Omega'' = {}^3/_2$ states ($X_2\ ^2\Delta_{3/2}$ and $W_1\ ^2\Pi_{3/2}$) have been extended likewise, to $v'' =$ 26 500 cm^{-1} above $v'' = 0$, $J = 2^1/_2$ in the ground state. Work is in progress to locate the more elusive $\Omega'' = {}^1/_2$ states whose influence is obvious in perturbations observed in X_1, X_2, and W_1 and whose energy levels remain key input for analysis of a system involving three heavily interacting electronic states.

Zeeman Spectrometry. The improvement in S/N ratios in the spectra have also made it possible to study Zeeman responses, when the line intensities are distributed over their several M_J components. Even close to Doppler-limited resolution, it is possible to resolve some of the Zeeman patterns in transition metal hydride species with modest magnetic fields. The magnetic response of NiH was studied by Field and co-workers[12,13] for some of the stronger electronic transitions by laser spectroscopy, scanning lasers across individual lines. High resolution resolved fluorescence can extend such studies to many transitions simultaneously. We have designed and optimized a magnetic circuit (using magnetic field simulation software, Vizimag[14]), which has been incorporated around the cold source, so that Zeeman splittings can be measured in controlled magnetic field conditions, either in excitation spectroscopy (transitions from the electronic ground state) or in FT resolved fluorescence. We used a simple geometry where the molecular "jet", the laser beam and the magnetic field are each on one of three perpendicular axes (Figure 7). In the first experiments, a coil (2000 turns, current $I_{DC} = 0-5$ A) produced a magnetic field in a ferrite with a pole diameter of 20 mm and a pole gap of 10 mm. This resulted in a homogeneous magnetic field in the pole gap, tunable from $B = 0$ to 0.15 T, in the region of the molecular flux. In such magnetic circuits, the lines of field are trapped within the ferrite (see the simulation in Figure 7) and "escape" into the gap, producing a field that varies crudely as the inverse of the gap width. In a second version, two permanent NdFeB magnets were simply attached magnetically to the edges of the gap, with no coil at all. A field of 0.7 T can be attained with a gap of 1 cm between the magnets.

The laser beam was gently focused by a two-lens telescope in the center of the gap. The laser polarization was oriented using a half-wave plate, either parallel to the magnetic field for π polarization or perpendicular for σ polarization. Backward fluorescence was collected on a pierced mirror and focused through a high-pass filter either onto a photomultiplier tube or onto the emission port of the FTS. In the first configuration, the laser beam was scanned in frequency and intensity-modulated with a mechanical chopper and the fluorescence signal was recorded on a digital oscilloscope via a lock-in amplifier. Frequency marker fringes and an iodine reference spectrum were recorded simultaneously, to obtain calibrated excitation spectra. Figure 8a shows the $Q(2^1/_2)$ $B^2\Delta_{5/2} \leftarrow X_1\ ^2\Delta_{5/2}(1-0)$ transitions for ^{58}NiH, ^{60}NiH, and ^{62}NiH recorded by excitation spectroscopy at low magnetic field with the electromagnet ($B = 0.13$ T), and at a stronger field strength with NdFeB magnets ($B = 0.67$ T). The isotope structure is resolved in both cases, but individual M_J components are not. Figure 8b illustrates the more complex patterns seen for the first P line ($P\ 3^1/_2$) of the same band, where individual M_J components are resolved, but where the isotopic transitions overlap one another.

In the second type of experiment, the laser was tuned to a chosen resonance, and the fluorescence spectrum was recorded using the FT spectrometer. With Brewster windows on the source, laser scatter was sufficiently low that the spectrum could be recorded without optical filters. Figure 9 illustrates a very small part of a FT spectrum of laser-induced fluorescence, recorded at 0.02 cm^{-1} resolution (330 coadded scans), in a magnetic field of 0.72 T, showing some

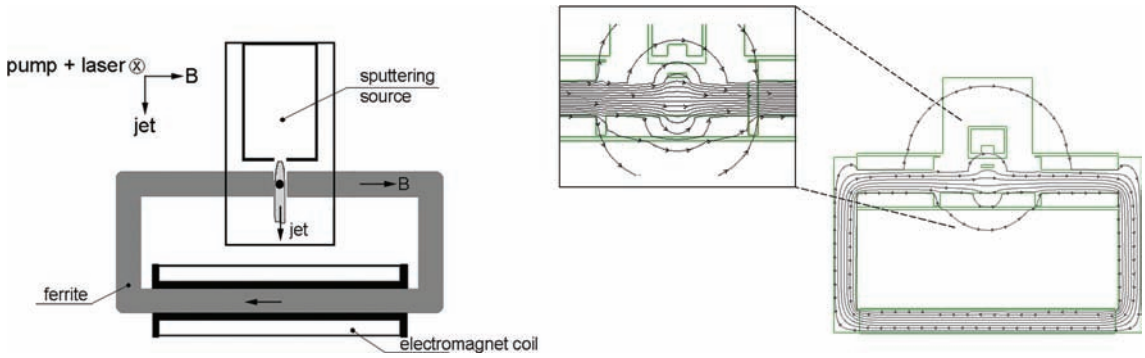

Figure 7. Ferromagnetic circuit: schematic diagram of the setup and magnetic field simulation. The inset shows an enlarged view between pole caps, calculated with a finer mesh to show the predicted field homogeneity in this region.

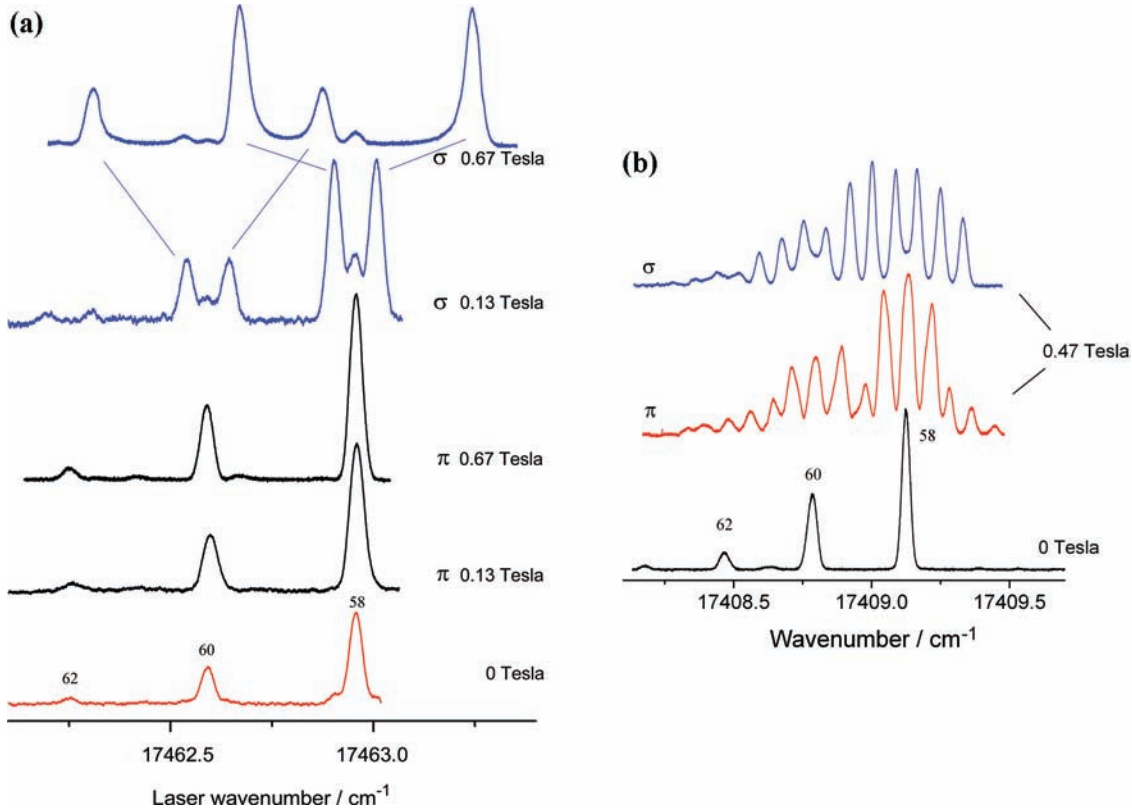

Figure 8. Zeeman spectra of NiH recorded in laser excitation (62 labels ^{62}NiH etc). (a) Q($2^1/_2$) B−X_1 (1−0), in field-free conditions (lowest trace), and at 0.13 and 0.67 T. Zeeman patterns are shown for π ($\Delta M_J = 0$) and σ ($\Delta M_J = \pm 1$) polarization. Individual components are not resolved. (b) The P($3^1/_2$) line of the B−X_1 transition shows fully resolved Zeeman patterns at 0.47 T.

collisionally induced transitions (F−X_1(0−0) and A−X_1(1−0) bands). The line profiles for Q and R lines are sufficiently different that it is easy to decide which lines belong to which branch. The lower trace shows an extract of the zero-field spectrum (Figure 4) for comparison: the S/N ratio is far better when all M_J components are superposed in the absence of magnetic field, and with only 50 coadded scans. The laser excited the σ^+ Q($2^1/_2$) B−X_1(1−0) transition in ^{58}NiH, and only this isotope is seen in the collisional bands. Dispersed fluorescence can thus discriminate isotopic structure, but (in the case of collisionally induced transitions) does not separate $\Delta M_J = 0$ from $\Delta M_J = \pm 1$ components. At 0.72 T, the M_J structure is at least partially resolved for many of the transitions shown in Figure 4.

The distinctive Zeeman patterns not only provide an obvious visual aid to assignment when several electronic transitions occur in the same spectral window but also offer a direct probe of the electronic configurations of a given state. The Zeeman splittings for the M_J sublevels are, to a first approximation, independent of rotational and vibrational constants, and, in Hund's case (a) coupling, are given by

$$E(J,M_J) = E_0 + \frac{\mu_B B g M_J \Omega}{J(J+1)} \qquad (4)$$

where μ_B is the Bohr magneton, 0.4669 cm^{-1}/T, and B is the magnetic field (Tesla). Rotational quantum numbers, J, and the total angular momentum quantum number, Ω, are unambiguously determined from rotational analysis. The molecular Landé factor, g, is determined from electronic orbital (Λ) and spin (Σ) quantum numbers: $g = \Lambda + 2.0023\Sigma$, and this quantity can allow some possible electronic state assignments to be eliminated if assignments are not obvious. The Zeeman patterns of the lowest rotational lines of the A($\Omega' = {}^5/_2$)−X_1 $^2\Delta_{5/2}$(1−0) band (shown in Figure 9) illustrate this quite well. The A−X_1

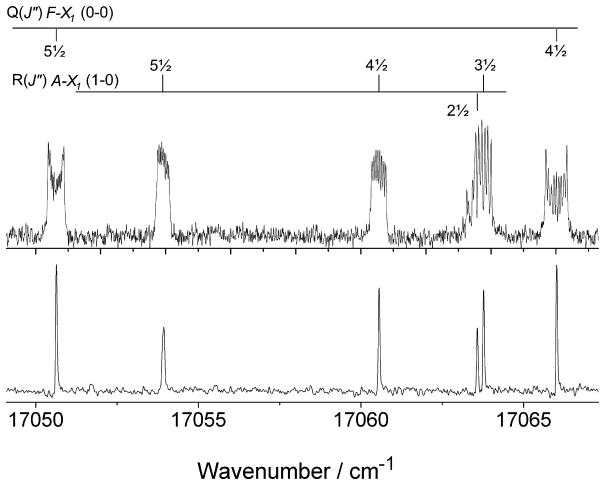

Figure 9. Upper trace: portion of the FT resolved fluorescence spectrum of ^{58}NiH, with a 0.72 T magnetic field. $P = 1.4$ Torr, $I = 150$ mA. Laser excitation line Q($2^1/_2$) B−X (1−0), $\sigma_L = 17\,462.937$ cm^{-1}. Resolution: 0.022 cm^{-1}. Total recording time ∼14 h (coaddition of 330 scans). The lower trace shows the same spectrum at zero field (50 scans).

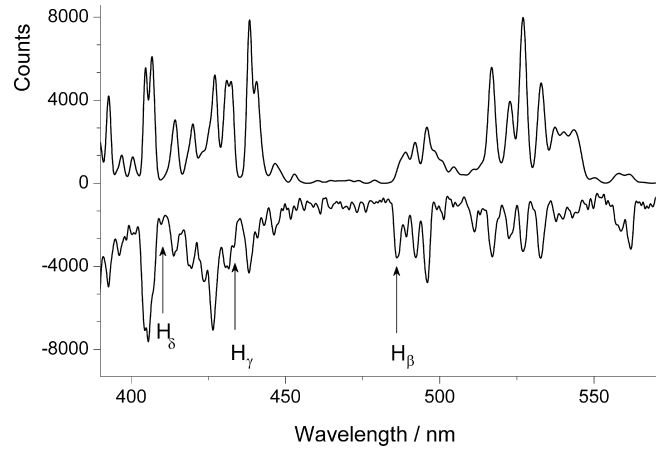

Figure 10. Low-resolution spectrum of the discharge spectrum obtained with an Fe cathode + 10% H_2 in argon (lower trace) and a reference spectrum for Fe I (upper trace).

bands we recorded at zero field show strong P and R branches with a weaker Q branch, which taken alone would suggest a $\Delta\Lambda = 0$ transition, with $\Lambda'' = 2$. However, the Zeeman patterns contradict this. We measure upper state Zeeman splittings in the $v = 1$, $J = 2^1/_2$ level of the A($\Omega' = {}^5/_2$) state ($T' = 17\,021.5$ cm^{-1}) to be 0.143, 0.222, and 0.270 cm^{-1} for field strengths of 0.48, 0.72, and 0.91 T, respectively, giving a g' value for $v = 1$ of the A state of 2.25(5), in agreement with literature values.[13] The A state could then derive from either $^4\Phi_{5/2}$ or $^2\Phi_{5/2}$ terms, whose Landé factors would be predicted close to 2. Only the quartet state is eligible, because ligand field calculations by Spain and Morse[15] have unambiguously correlated the $^2\Phi_{5/2}$ state of NiH with the G($\Omega' = {}^5/_2$) state, whose term energy $T'_{(v=0,J=2\,1/2)} = 18\,424.9$ cm^{-1}, is higher (as expected) than the term energy ($T'_{(v=0,J=3\,1/2)} = 17\,132.4$ cm^{-1}) of the F $^2\Phi_{7/2}$ state. This invalidates an earlier assignment for the A $^2\Lambda_{5/2}$ state (from Gray and Field[16]) as $^4\Pi_{5/2}$ but is nicely consistent with the ligand field calculations,[15] which reported 72% $^4\Phi$ + 12% $^4\Delta$ Φ + 8% $^2\Delta$ character for $v = 0$ of the A ($\Omega = {}^5/_2$) state, and also with recent ab initio calculations by Zou and Liu,[17] which list dominant configurations as 77% $^4\Phi$ + 22% $^2\Delta$ for the fifth highest $\Omega = {}^5/_2$ level.

High resolution FT spectroscopy offers at least three advantages for Zeeman spectroscopy to compensate the long recording times it requires: (1) isotopic selectivity with the cw single-mode laser; (2) broad spectral observation windows (typically 5000 cm^{-1}), allowing simultaneous detection of numerous systems and bands under the same (a priori stable) experimental conditions; and (3) automatic and self-consistent calibration for (in this instance) hundreds of spectral features.

Caveat. The obvious ways to separate overlapped Zeeman components are to increase the magnetic field B or the spectral resolution (or both). The NdFeB magnets we are using limit the magnetic fields we can produce (1 T when the pole gap is reduced to ∼4 mm), and our excitation spectra have Doppler-limited resolution. (The Fourier transform spectra actually showed marginally narrower linewidths than the excitation spectra, as velocity groups close to the Doppler profile maximum had been selected, but linewidths are still around 0.022 cm^{-1} (0.73 GHz).) Improvement in resolution should be possible by working in sub-Doppler conditions. An attempt to record excitation spectra at sub-Doppler resolution by intermodulated fluorescence spectroscopy[13] (IMF) was rather disappointing. An IMF experiment with two counterpropagating beams mechanically chopped at two indivisible frequencies, ω_1 and ω_2, followed by detection of the LIF at $\omega_1 + \omega_2$, gave only a 30% improvement in the fwhm linewidths: 0.7 GHz, compared with 1.0 GHz measured in the Doppler regime. We suspect that this limitation comes from a combination of operational pressure (around 1 Torr) and power broadening, as the minimum laser power required for fluorescence detection was 40 mW on each beam. We deduce that our source is not well suited to this application.

4. Production of FeH and Detection by Laser Excitation Spectroscopy. Low resolution discharge spectra similar to those obtained with nickel have been recorded from an iron cathode, using the same 10% H_2/Ar gas mix. The current in the discharge was 150 mA, running at a pressure of 1.4 Torr, with a flow rate of 45 sccm and a temperature of 34 °C, measured with a thermocouple situated outside the discharge. The lower trace in Figure 10 shows the spectrum from our discharge in a region containing Fe I lines, recorded on an AvaSpec-2048 Fiber Optic Spectrometer, with a 75 mm Czerny-Turner grating (300 lines/mm) at an instrumental resolution 2.4 nm. The upper trace is a reference spectrum, calculated by convolution of a high-resolution spectrum (recorded at Imperial College London in 1988[18]), with a 2.4 nm fwhm Gaussian profile. At first glance, the spectra are somewhat dissimilar. As with the nickel cathode in the presence of hydrogen, the H_β Balmer line is clearly visible from our source, and does not appear in the reference spectrum, and the relative intensities of the Fe lines differ. These discrepancies are probably related to the differences in the operational conditions: the discharge is produced in Ar/H_2 instead of Ne as in the reference spectrum. It is nevertheless clear that both Fe and H atoms are produced in our discharge and are expected to form FeH radicals in the gas phase.

A Coherent CR-899 cw Ti:Sa laser, equipped with medium wave optics and two intracavity etalons for single frequency operation, was used to excite the FeH F−X(1−0) band near 880 nm. A Burleigh WA1500 high-resolution wavemeter monitored the (manual) tuning of the laser to the desired rotational line. The laser beam was mechanically chopped, and the broadband LIF signal was detected by a silicon amplified photodetector (Thorlabs PDA36A) through a side window. A lens focused the intersection region between the laser beam and the molecular "jet", situated 20 mm below the anode, on the photocell. A high-pass filter removed the visible part of this

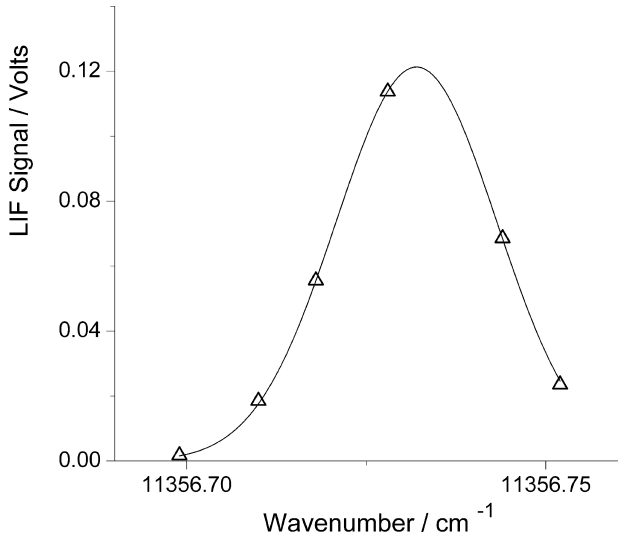

Figure 11. Measured laser excitation profile of the $Q_{ab}(3^1/_2)$ (1−0) F $^4\Delta_{7/2}$−X $^4\Delta_{7/2}$ line in FeH, centered at σ_L = 11 356.73 cm^{-1}. The line represents the fit of data points to a Gaussian function.

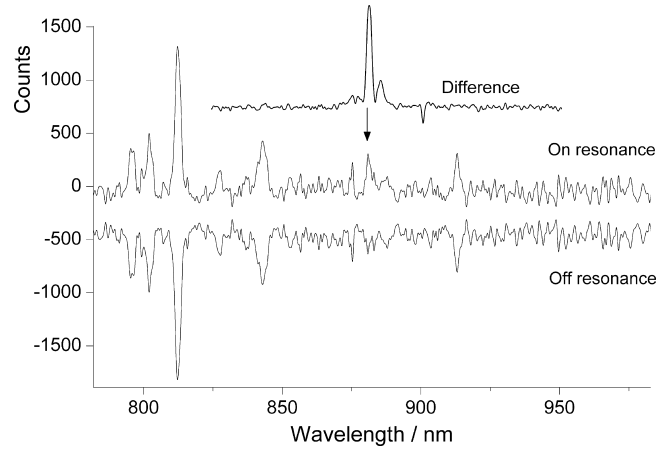

Figure 12. Emission spectra recorded on the low-resolution grating spectrometer. The laser on resonance 11 356.726 cm^{-1} (middle trace) and 0.015 cm^{-1} below resonance (lower trace, drawn as a negative signal) are noisy. Taking the difference between them clearly reveals a resonance fluorescence signal (the upper trace is drawn to the same wavelength scale as the other two, vertical scale is 0−210 counts). Laser power = 330 mW.

discharge, and a lock-in amplifier demodulated the signal at the chopping frequency to reduce residual noise. The laser (300 mW) was tuned to various rotational lines (for which accurate frequencies are known from the FT work of Phillips et al.[19]), in $\Delta\Omega = 0$ sub-bands of the F−X(1−0) band, with $\Omega = {}^1/_2$, $1^1/_2$, $2^1/_2$, $3^1/_2$, and $J \leq 6^1/_2$. The resonances were detected with a typical signal/noise ratio of 10. The optimal source conditions were 992 V, 300 mA, flow rate = 45 sccm, gas temperature = 38 °C, and P = 1.2 Torr. The excitation spectra were not recorded in any digital form, because the laser was not continuously tunable. Tuning manually, we measured (stepwise) the profile of the strongest transition in this region of the FeH spectrum, namely $Q_{ab}(3^1/_2)$ of the $^4\Delta_{7/2}$−$^4\Delta_{7/2}$ sub-band (Figure 11), and estimated the fwhm linewidth to be 0.026(1) cm^{-1} by fitting to a Gaussian function. This linewidth is comparable to the calculated Doppler width at 38 °C of 0.020 cm^{-1}. Taking into account the sensitivity of the detector and the geometry of the optical collection of the LIF, the absorption coefficient is estimated to be $\Delta I/I \sim 3 \times 10^{-6}$ cm^{-1}.

We recorded two spectra at slightly different laser frequencies with the grating spectrometer, one at resonance and the other offset by 0.015 cm^{-1}. The spectra are quite noisy, but an FeH line F−X(1−0) is very obvious when the "off resonance" spectrum is subtracted from the first one (Figure 12). The Ar I emission background is largely eliminated, together with much of the noise. These preliminary results establish that FeH is being detected from a sputtering source, in itself a novel result. Earlier work by Phillips used a high-temperature furnace,[19] and recent studies by Brown and Steimle and co-workers either formed FeH in cold conditions, by laser ablation,[20,21] or at ambient temperatures, by reacting iron pentacarbonyl with hydrogen atoms formed in a microwave discharge.[22,23] Given that the (0−0) band at 989 nm has a Franck−Condon factor about 1 order of magnitude larger[24] than for the (1−0) transition we have investigated, and that no multipass arrangement has been used in this experiment, stronger iron monohydride signals than this should be within reach. For absorption studies, another setup has been successfully explored by the group of Field at MIT: a long-pass discharge surrounded by a magnetic confinement coil.[25] This sort of arrangement is promising for future experiments using intracavity absorption spectroscopy to enhance sensitivity.

Conclusion

We describe a compact molecular source for nonvolatile radicals, adapted to work in emission, and to allow laser-induced fluorescence to be recorded with a standard "on the fly" Fourier transform spectrometer. Fourier transform spectroscopy offers an attractive combination of high resolution, spectral coverage, and relative intensity accuracy but is demanding in its requirement of strong signals that are free of amplitude noise. This disqualifies many of the molecule-generation sources used in pulsed molecular beam + pulsed laser spectroscopy to study metal-containing species. Ablation sources are ubiquitous and have been used to generate a wide range of transient species, but they are inappropriate for use with an FT spectrometer, partly because of very low repetition rates leading to excessive data acquisition times, and partly because of unreliable pulse-to-pulse repeatability of ablation. While discharges usually work well with FT methods when using gas phase (or volatile) precursor species to generate emission spectra of ions and neutrals, they can prove problematic when random amplitude noise (generated by sparks from the electrodes for example) is converted into frequency noise in the spectrum. Metal-based discharges are consequently widely used in pulsed laser experiments but are uncommonly used with Fourier spectrometers, for which extended recording times are required. The notable exception to this is the combination of high-temperature furnace plus electrical discharge, used in recent years at the University of Waterloo for the study of transition metal halides including, for example, NiF[26] and CoCl,[27] in which the nonvolatile precursors are vaporised thermally. We believe that our more compact hollow cathode discharge source, optimized for use with FT spectrometers and dispersed fluorescence, holds promise for the future study of a wide range of transient molecules, and especially of metal hydrides and oxides. It also offers an alternative to volatile but toxic precursors such as metal carbonyls[28] (as used for example in recent investigations on FeH[29,30]) for small-scale laboratory investigations.

Acknowledgment. We thank Dr. E. J. Friedman-Hill (Sandia National Lab) for much useful information concerning the original design of the "hot source". We are indebted to B. Erba and M. Néri (LASIM) for technical suggestions and for the

construction of the discharge source. We thank Dr. A.-M. Jurdyc (UMR 5620 Université Lyon 1 & CNRS) for the loan of the Ti:Sapphire laser used to investigate FeH. We are glad to acknowledge financial support from the Agence Nationale de la Recherche (France) ANR-08-BLAN-0017-01, from the CNRS-Royal Society exchange programme, and (for R.W.F.) from NSF, grant CHE-0749821.

References and Notes

(1) Donati, J. F.; Brown, S. F. *Astron. Astrophys.* **1997**, *326*, 1135.
(2) Gray, J. A.; Li, M.; Nelis, T.; Field, R. W. *J. Chem. Phys.* **1991**, *95*, 7164.
(3) Vallon, R.; Richard, C.; Crozet, P.; Wannous, G.; Ross, A. J. *Astrophys. J.* **2009**, *695*, 00.
(4) Vallon, R. Thèse de Doctorat, Université Lyon 1, 2007.
(5) Friedman-Hill, E. J. Ph.D. thesis, Massachusetts Institute of Technology, 1992.
(6) Ralchenko, Y.; Kramida, A. E.; Reader, J. NIST_ASD_Team. NIST Atomic Spectra Database (version 3.1.5), [Online]. Available: http://physics.nist.gov/asd3, 2008.
(7) Herzberg, G. *Molecular Spectra and Molecular Structure I: Spectra of Diatomic Molecules*, 2nd ed.; Van Nostrand Reinhold: New York, 1950.
(8) Hodoroaba, V. D.; Steers, E. B. M.; Hoffmann, V.; Wetzig, K. *J. Anal. Atom. Spectrom.* **2001**, *16*, 43.
(9) Gray, J. A. Ph.D. thesis, MIT, 1988.
(10) Vallon, R.; Crozet, P.; Ross, A. J. *J. Phys. IV* **2006**, *135*, 289.
(11) Budtz-Jørgensen, C. V.; Kringhøj, P.; Bottiger, J. *Surface Coatings Technol.* **1999**, *116*, 938.
(12) Gray, J. A.; Li, M. G.; Field, R. W. *J. Chem. Phys.* **1990**, *92*, 4651.
(13) McCarthy, M. C.; Kanamori, H.; Steimle, T. C.; Li, M. G.; Field, R. W. *J. Chem. Phys.* **1997**, *107*, 4179.
(14) Beeteson, J. S. Vizimag, Magnetic field software, http://www.vizimag.com.
(15) Spain, E. M.; Morse, M. D. *J. Chem. Phys.* **1992**, *97*, 4641.
(16) Gray, J. A.; Field, R. W. *J. Chem. Phys.* **1986**, *84*, 1041.
(17) Zou, W. L.; Liu, W. J. *J. Comput. Chem.* **2007**, *28*, 2286.
(18) Learner, R. C. M.; Thorne, A. P. *J. Opt. Soc. Am. B* **1988**, *5*, 2045.
(19) Phillips, J. G.; Davis, S. P.; Lindgren, B.; Balfour, W. J. *Astrophys. J. Supp. Ser.* **1987**, *65*, 721.
(20) Harrison, J. J.; Brown, J. M.; Chen, J.; Steimle, T. C.; Sears, T. J. *Astrophys. J.* **2008**, *679*, 854.
(21) Steimle, T. C.; Chen, J. H.; Harrison, J. J.; Brown, J. M. *J. Chem. Phys.* **2006**, *124*.
(22) Fletcher, D. A.; Carter, R. T.; Brown, J. M.; Steimle, T. C. *J. Chem. Phys.* **1990**, *93*, 9192.
(23) Goodridge, D. M.; Carter, R. T.; Brown, J. M.; Steimle, T. C. *J. Chem. Phys.* **1997**, *106*, 4823.
(24) Dulick, M.; Bauschlicher, C. W.; Burrows, A.; Sharp, C. M.; Ram, R. S.; Bernath, P. *Astrophys. J.* **2003**, *594*, 651.
(25) Li, M. G.; Gray, J. A.; Field, R. W. *Chem. Phys.* **1987**, *117*, 171.
(26) Pinchemel, B.; Hirao, T.; Bernath, P. F. *J. Mol. Spectrosc.* **2003**, *215*, 262.
(27) Ram, R. S.; Gordon, I.; Hirao, T.; Yu, S.; Bernath, P. F.; Pinchemel, B. *J. Mol. Spectrosc.* **2007**, *243*, 69.
(28) Beaton, S. P.; Evenson, K. M.; Nelis, T.; Brown, J. M. *J. Chem. Phys.* **1988**, *89*, 4446.
(29) Goodridge, D. M.; Carter, R. T.; Brown, J. M.; Steimle, T. *J. Chem. Phys.* **1997**, *106*, 4823.
(30) Wilson, C.; Brown, J. M. *J. Mol. Spectrosc.* **2001**, *209*, 192.

JP9033968